energies

MDPI

Article

Water Recuperation from Hydrogen Fuel Cell during Aerial Mission

Lev Zakhvatkin [1,*], Alex Schechter [2] and Idit Avrahami [1]

[1] Department of Mechanical Engineering and Mechatronics, Ariel University, P.O. Box 3, Ariel 44837, Israel
[2] Department of Chemical Sciences, Ariel University, P.O. Box 3, Ariel 44837, Israel
* Correspondence: levz@ariel.ac.il

Abstract: A water recuperation system (WRS) from an open-cathode proton exchange membrane fuel cell (PEMFC) is designed to increase the energy density of hydrogen production by hydrolysis of metal hydrides. WRS may significantly reduce the water weight in the carried fuel. The design is based on circulating the humid air through the PEMFC stack in a closed dome. To ensure oxygen supply to the PEMFC, the WRS has a ventilation inlet and an exhaust outlet. The required conditions for ventilation flow are developed theoretically and examined experimentally in a WRS prototype with a commercial PEMFC at 20–100 W. The experimental system includeds a closed dome, an edge cooling system for the PEMFC, a controllable ventilation air inlet, and an exhaust port. The humid exhaust air was cooled down to the ambient temperature to improve vapor condensation. Results show high efficiency (80% recuperated water from prediction), with a potential to achieve gravimetric hydrogen storage capacity (GHSC) of >6 wt% at an ambient temperature of 27 °C. The described principle may be applied for small fixed-wing drones where the cold ambient air may be utilized both for providing oxygen supply and for thermal management of the PEMFC and the humid exhaust, thus allowing higher GHSC.

Keywords: hydrogen generation; metal hydrides; fuel cells; water recuperation; water recovery; drones; proton exchange membrane; energy density; gravimetric hydrogen storage capacity; vapor condensation

check for updates

Citation: Zakhvatkin, L.; Schechter, A.; Avrahami, I. Water Recuperation from Hydrogen Fuel Cell during Aerial Mission. *Energies* **2022**, *15*, 6848. https://doi.org/10.3390/en15186848

Academic Editor: Ivan Tolj

Received: 18 August 2022
Accepted: 11 September 2022
Published: 19 September 2022

Publisher's Note: MDPI stays neutral with regard to jurisdictional claims in published maps and institutional affiliations.

Copyright: © 2022 by the authors. Licensee MDPI, Basel, Switzerland. This article is an open access article distributed under the terms and conditions of the Creative Commons Attribution (CC BY) license (https://creativecommons.org/licenses/by/4.0/).

1. Introduction

Hydrogen fuel cell (FC) is one of the prospective development directions of energy sources when considering portable devices. FCs convert chemical energy from hydrogen gas (H_2) to electrical energy, heat, and water vapor. It has zero CO_2 emission and can produce three times more energy than gasoline per unit of mass in combustion engines [1,2].

If coupled with renewable but unstable energy sources, such as wind or solar power plants, and green energy storage/generating systems, e.g., FCs, may greatly improve the utilization rate and stability of renewable energy [3]. Among all types of FCs, such as solid-oxide, alkaline, and molten carbonate FCs [4], proton exchange membrane fuel cells (PEMFCs) are considered suitable for transportation and portable applications due to low operation temperature/pressure ranges (45–100 °C/0.4–0.5 bar hydrogen) and fast start-up time [5].

There are some shortcomings of PEMFCs associated with high materials cost, manufacturing price, and limited lifetime that limit the commercialization of this technology. However, the most challenging barrier for mobile applications is hydrogen storage [2,6]. The US Department of Energy (DOE) set a target for the energy density of a hydrogen storage system of 1800 Wh/kg or 5.4 wt% gravimetric hydrogen storage capacity (GHSC) for automotive applications by 2025 [7]. Currently, only a limited safety solution of H_2 storage at 700 bars in special tanks or complex storage using liquid hydrogen or absorbed hydrogen has been shown to provide a storage density of 4.0–5.7 wt% [8,9]. However, pressurized or complex storage is not suitable for most of the needs, and further search for alternatives is required.

Metal hydrides have the potential for meeting those targets [1,10,11]. For example, sodium borohydride (SBH, $NaBH_4$) is a common candidate since it has high hydrogen content, is well studied, has relatively low cost, is stable as a solid in dry air for months, its reaction products are non-toxic, and it can be recycled [12]. The fuel comprised of SBH, and H_2O can theoretically deliver 10.8 wt% of Hydrogen [13]. Notably, H_2O provides half of the H_2 produced by the reaction (Equation (1) below), whereas the rest comes from the SBH. This reaction, however, faces different hurdles. The main challenges are the low solubility of SBH and its product, sodium metaborate ($NaBO_2$), in water, which implies that an excess amount of water is needed to facilitate the reaction and solubilize its products [6,13–15]. In a previous study, we suggested an efficient method of hydrogen generation by catalytic reaction between solid SBH and water, which allows the utilization of recuperated water for further hydrogen production [16].

Usual commercially available open cathode FCs produce water in the state of vapor and the flow forced through them by the fan plays a dual role: cooling and oxygen supply. The membrane electrode assemblies (MEAs) of such stacks are designed to operate at much higher ventilation flow rates than stacks with a close cathode (>300 times higher), since the cooling flow greatly exceeds the stoichiometric amount of air required for stable operation [13].

Implementation of a water recuperation system (WRS) that harvests water vapor from the FC cathode emission and recirculates it into the generator may significantly reduce the weight of the carried water, hence increasing the fuel's GHSC, since a part of the required excess water is not stored anywhere but appears during FC operation. Previous attempts to use water vapor directly from the FC were made by Kong et al. [14]. However, they observed that SBH did not react well with water vapor. Therefore, an alternative method should be applied to exploit water vapor from the FC, e.g., by water condensation and collection for further implementation in the hydrogen generator. Several studies were performed regarding water recuperation from hydrogen fuel cells. Yamazaki et al. [17] developed an analytical model which predicts the amount of recuperated water from the PEMFC and proved it experimentally. Tibaquirá et al. [18] examined if such recuperated water meets the sufficient requirements for drinking water. Anand et al. [19] proposed using a water separator for a more efficient recuperation. Nevertheless, all these studies were performed in closed-cathode FCs which require much lower air supply and are considered suitable for high-power fuel cells (1–2 kW and above). Portable applications (30–1000 W) use FC stacks with cathode open to the air, which are of much greater interest [20,21] due to their capability to reduce the weight, volume, cost, and control complexity. In the open cathode FC, the oxidation flow is coupled with the cooling flow. Hence, the required airflow is much higher than those of closed cathode stacks, and water cannot be condensed just by cooling the exhaust flow. Therefore, to condensate water from an open-cathode FC, a more complex system is required with a partially closed air recirculation. As far as we know, no WRS as proposed here was suggested, developed, and tested before.

Among the different types of FC-based systems which can benefit from an SBH hydrogen generator with high GHSC, small unmanned aerial vehicles (UAVs), also called drones, are of special interest. It was shown [19] that utilizing an FC power plant may significantly increase their flight duration. For example, a 10 kg fixed-wing drone can be powered by a 200 W FC, which makes this kind of vehicle suitable for further research [22]. However, the FC should be isolated from the cold and dry ambient air at high altitudes to prevent FC power output degradation due to dehydration or overcooling. In these cases, the cold ambient air can be utilized for FC edge cooling (i.e., removing heat by radiators connected to the FC's edges, as described in one of our previous research articles [23]), as well as for the implementation of a WRS from FC vapor for hydrogen production. This may significantly increase the energy density of the power plant fueled by solid SBH.

In this study, we suggest utilizing the passing ambient airflow both as an oxygen source for ventilation and as the carrier for convection cooling—for both FC thermal management (via edge cooling) and for condensing the FC vapor. For this purpose, we

examined enclosing the FC in a closed dome and recirculating the humid air through the stack while using edge-cooling methods for FCs thermal management [23]. To provide sufficient oxygen for FC operation, the dome includes a ventilation inlet and exhaust outlet ports (Figure 1).

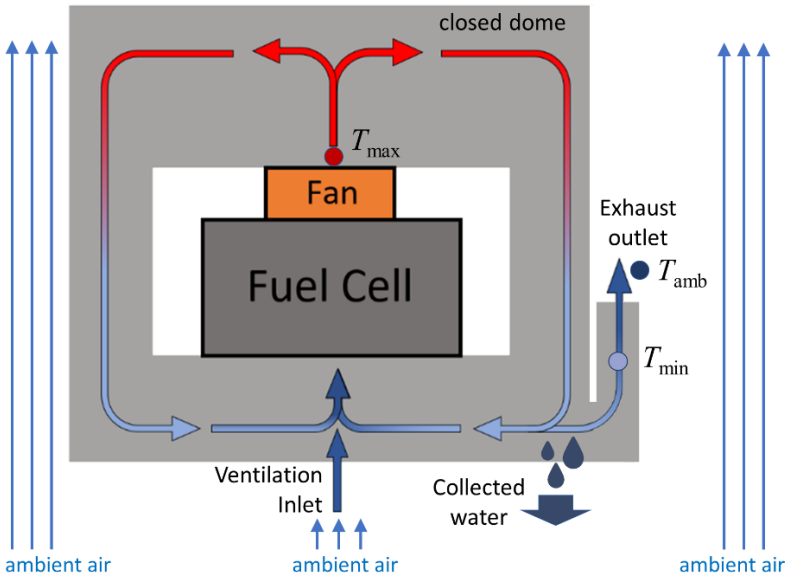

Figure 1. A schematic description of the WRS with the recirculating air in the dome's internal channels, including the fuel cell, the fan, and the inlet ventilation and outlet exhaust ports.

A controlled ventilation airflow is forced through the ventilation inlet at the desired flow rate. It mixes with air already circulating inside the system (by a fan) and reduces its humidity. It is further supplied to the FC where a part of the oxygen molecules reacts at the MEA's cathode side catalyst layer [24] with hydrogen ions and electrons from the circuit to produce electrical current and turns into water molecules [25]. Hydrogen ions, in their turn, are supplied there through proton exchange membrane (usually Nafion) after the catalytical split of hydrogen molecules to protons and electrons at the MEA's anode.

The air heats up while flowing through the FC, so the relative humidity (RH) of the heated air inside the stack is expected to be low enough to prevent MEA flooding by active condensation. The hot humid air (T_{max} in Figure 1) that leaves the FC, circulates in the WRS dome by a fan and cools down on the way (over the dome's walls by the ambient air), while a small part of it leaves the system as exhaust (due to mass conservation). The outlet exhaust air flows through a heat exchanger and cools down to ambient (or close to ambient) temperature (T_{min} at Figure 1), where a dew point is reached, and condensation occurs on the inner walls of the dome. This way, most of the vapor produced by the FC is condensed and collected (by gravity) from the enclosed dome and delivered to the generator for further H_2 production.

The optimal flow rate of the ventilation air can be estimated analytically. The ventilation flow should be sufficient for FCs' stable performance but not too high to minimize vapor losses through the exhaust. In addition, to prevent the membrane from flooding and the consequent decrease in FC performance at full saturation conditions, the actual ventilation airflow rate should be examined experimentally. Therefore, in this manuscript, we develop an analytical description of the condition in which this concept might be employed. A theoretical expression for the ventilation flow rates as a function of FC power and ambient temperature and humidity is offered. An experimental prototype was built and tested to validate the theoretical calculations, prove the concept's feasibility, and estimate its efficiency at relatively low temperature gradient (i.e., at room temperature). Note that high altitude conditions are expected to further improve the water collection efficiency and system energy density, as predicted by the theoretical calculations.

2. Analytical Model

In this section, we provide a theoretical calculation of the expected improvement in hydrogen storage efficiency and conditions at which the WRS should operate. The process of hydrogen production from SBH hydrolysis at the H_2 generator is given by Equation (1):

$$NaBH_4(s) + (2+x)H_2O(l) \rightarrow NaBO_2nH_2O(l) + 4H_2(g) + (x-n)H_2O \quad (1)$$

where x is the excess of water and $n \leq x$ is the hydration water trapped by $NaBO_2$ molecules, which varies with solution temperature. For reaction temperatures lower than 53.6 °C, n = 4. For a temperature range between 53.6 °C and 105 °C (as in our case), n = 2. At temperatures above 105 °C, n = 0.5 [6].

The electrochemical reaction that takes place in the FC is given by Equation (2):

$$2H_2(g) + O_2(g) \rightarrow 2H_2O(g) \quad (2)$$

Two parameters are commonly utilized to describe FC power plant fuel efficiency: GHSC and energy density. Increased GHSC means increased fuel energy density and vice versa. All the calculations in this research are presented in terms of fuel GHSC defined in Equation (3):

$$GHSC = \frac{m_{H_2}}{m_{fuel}} \cdot 100\% \quad (3)$$

where m_{fuel} is the mass of fuel (water + SBH). The actual value of m_{fuel} changes during operation if a WRS is utilized.

$$m_{fuel} = m_{SBH} + m_{H_2O}^{req} - m_{H_2O}^{coll} \quad (4)$$

m_{SBH}, $m_{H_2O}^{req}$, and $m_{H_2O}^{coll}$ are the initial mass of SBH powder, the total mass of water required to fully accomplish the reaction, and the total mass of water collected from the WRS, accordingly.

$$m_{SBH} = \frac{1}{4} m_{H_2} \frac{M_{SBH}}{M_{H_2}} = \frac{37.8}{4 \cdot 2} m_{H_2} = 4.73 m_{H_2} \quad (5)$$

$$m_{H_2O}^{req} = \frac{(2+x)}{4} m_{H_2} \frac{M_{H_2O}}{M_{H_2}} = \frac{18}{2 \cdot 4}(2+x) = 2.25(2+x) m_{H_2} \quad (6)$$

and $m_{H_2O}^{coll}$ can be represented in the following view:

$$m_{H_2O}^{coll} = k\left(m_{H_2O}^{prod} + m_{H_2O}^{in}\right) = k\left(\frac{M_{H_2O}}{M_{H_2}} m_{H_2} + m_{H_2O}^{in}\right) = k\left(9 m_{H_2} + m_{H_2O}^{in}\right) \quad (7)$$

where k is the coefficient of water collection out of the total amount of water that appeared inside the WRS and water carried by ventilation flow ($m_{H_2O}^{prod} + m_{H_2O}^{in}$). $m_{H_2O}^{prod}$ represents the amount of water formed in the FC cathode during the oxygen reduction, and $m_{H_2O}^{in}$ represents the amount of water entering the WRS with the ambient ventilation air (see Figure 1).

Substituting Equations (4)–(6) to Equation (3) gives the following expression for average fuel GHSC:

$$GHSC = \frac{2}{9.23 + 2.25x - k\left(9 + \frac{m_{H_2O}^{in}}{m_{H_2}}\right)} \cdot 100\% \quad (8)$$

In our previous research [16], we were able to achieve a water excess x of 6.4 using a novel generator that used solid SBH powder. That way, for the worst case, where the inlet air is totally dry (i.e., $m_{H_2O}^{in}$ = 0), GHSC becomes:

$$GHSC = \frac{1}{23.63 - 9k} \cdot 100\% \quad (9)$$

The suggested WRS should reduce the initial mass of excess water stored in the generator (according to k), while keeping the required water excess for the reaction. Recuperation alone, however, will not be able to increase GHSC significantly if the products of $NaBO_2$ with excess water remain inside the system throughout the operation cycle. Fortunately, $NaBO_2$ water solution is non-toxic [6,13] and can be purged to the ambient environment. That way the fuel's weight in the system can reach zero by the end of the process.

Figure 2 shows the influence of the water collection coefficient on GHSC of initially stored fuel described by Equation (8). It is shown that water recuperation from the FC even in the absence of water vapor supply from the ambient air can increase the GHSC of stored fuel up to 38%. The actual increase of the whole energy system's GHSC, however, will also depend on the weight of the WRS, including FCs heat management and its water collection properties.

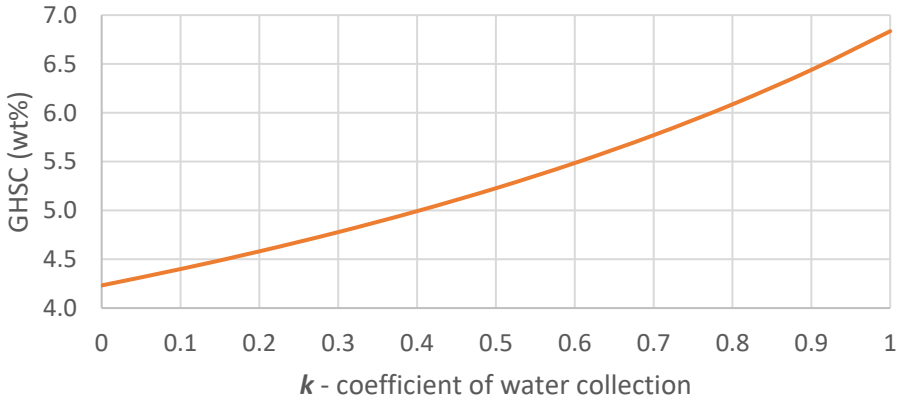

Figure 2. GHSC of the initial SBH–water mixture as a function of k for hydrogen generator with x = 6.4.

To implement the recuperation approach, one should first define the optimal ventilation airflow sufficient for stack stable operation, estimate the humidity level which may be achieved in that flow, and make sure that its dew point is higher than ambient temperature. In that case, condensation and, accordingly, recuperation is possible. The mass of water produced by FC ($\dot{m}^{prod}_{H_2O}$) can be found from Faraday's laws of electrolysis:

$$\dot{m}^{prod}_{H_2O} = \dot{n}^{prod}_{H_2O} M_{H_2O} = \frac{INM_{H_2O}}{2F} \tag{10}$$

where $\dot{m}^{prod}_{H_2O}$ and $\dot{n}^{prod}_{H_2O}$ are water mass and molar flows, M_{H_2O} = 18 g/mol is the molar mass of water, I is stacks current (in Ampere), N is the number of MEAs in the stack, and F = 96,500 (C/mol) is the Faraday constant.

The corresponding stoichiometric ventilation airflow $\dot{V}_\lambda$ is:

$$\dot{V}_\lambda = V_m \frac{IN}{0.21 \cdot 4F} \tag{11}$$

where V_m is air molar volume calculated from the ideal gas equation. The number 0.21 stands for the molar percentage of oxygen in the air. The required airflow $\dot{V}_{in}$ can be calculated using:

$$\dot{V}_{in} = \lambda V_m \frac{IN}{0.21 \cdot 4F}; \; \lambda = \frac{\dot{V}_{in}}{\dot{V}_\lambda} > 1 \tag{12}$$

where $\lambda > 1$ is the ratio between the actual airflow and stoichiometric air flow rate required for stable FC operation. In this paper, we define stoichiometry of the ventilation flow as the ratio between the actual ventilation flow to theoretical sufficient to fully accomplish an electrochemical reaction inside the stack: 1 mole of oxygen for every 2 moles of supplied hydrogen, assuming that the molar fraction of oxygen in the air is 21%.

If the ventilation airflow $\dot{V}_{in}$ is too high, the absolute humidity (AH) inside the system may become too low to achieve a dew point at the exhaust cooled down to T_{min} (Figure 1), and condensation conditions might not be obtained in the system. To ensure water collection, the mass of water vapor that leaves the system through exhaust ($\dot{m}^{out}_{H_2O}$) should be less than the total amount of water produced by the FC plus water that entered the system through ventilation. $\dot{m}^{out}_{H_2O}$ can be found from the following equation:

$$\dot{m}^{out}_{H_2O} = AH_{sat}(T_{min}) \cdot \dot{V}_{out} \tag{13}$$

where the absolute humidity at saturation AH_{sat} is defined as follows:

$$AH_{sat} = \frac{e_s(T)}{R_v T} \tag{14}$$

where $e_s(T)$ is the saturated vapor partial pressure and R_v = 461 J/kg*K is the specific gas constant for water vapor.

Since the FC consumes a part of the oxygen molecules and increases the flow humidity, the outlet flow $\dot{V}_{out}$ is different from the ventilation inflow and should be found (from mass conservation). Assuming that the flow is cooled down to T_{min}, and the sum of air and vapor partial pressures are equal to atmospheric and using the ideal gas equation, $\dot{V}_{out}$ can be presented in the following view:

$$\dot{V}_{out} = \frac{\left(1 - \frac{0.21}{\lambda}\right) P_{atm} \dot{V}_{in}}{P_{atm} - e_s(T_{min})} \tag{15}$$

Water vapor partial pressure at saturation (e_s) can be found from Tetens' equation (temperature in degrees Celsius):

$$e_s(T) = 0.61078 \cdot \exp\left(\frac{17.27T}{T + 237.3}\right) \tag{16}$$

Assuming the worst-case scenario, using dry inlet air ($m^{in}_{H_2O} = 0$), the ratio between produced water by the FC and lost water through exhaust outflow can be found from Equations (10), (12), (14) and (16):

$$\gamma > 1 \Rightarrow \lambda < \frac{7.56(P_{atm} - e_s(T_{min}))}{AH_{sat}(T_{min}) P_{atm} V_m} + 0.21 \tag{17}$$

Thus, while the inlet ventilation flow stoichiometry satisfies the following equation, the FC has enough oxygen to operate, while condensation in the WRS is ensured.

$$1 < \lambda < \frac{7.56(P_{atm} - e_s(T_{min}))}{AH_{sat}(T_{min}) P_{atm} V_m} + 0.21 \tag{18}$$

Figure 3 presents the threshold of stoichiometry coefficient λ *(T)* at the dew point for flight at (−20 °C) > $T_{\min}$ > 35 °C and for air pressure of P_{atm} = 1 atm (as recommended for FC operation). Ventilation airflow with stoichiometry λ that lies between the red and blue lines should be sufficient for both FC operation and condensation.

It is clear from Figure 3 that for $T_{\min}$ < 35 °C, the FC produces a higher amount of water than required for saturation at the stoichiometric air inflow (l = 1). For lower exhaust temperatures (e.g., cooling down to an ambient temperature at high altitudes), the saturation can be achieved at higher inlet flow, with up to λ = 340 at $T_{\min}$ = −20 °C. Therefore, the actual amount of recuperated water depends on several parameters, including the FC operating conditions (current and temperature), surrounding humidity and temperature of inflow, and the humidity and temperature of outflow.

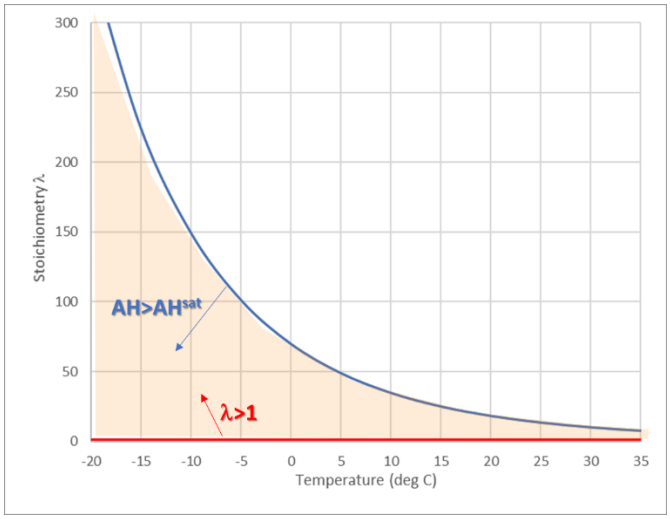

Figure 3. Sufficient stoichiometry airflow for both FC operation (red line) and obtaining a fully saturated air (blue line) as a function of minimal air temperature in the WRS.

To estimate the part of recuperated water (k), the following assumptions are applied: the airflow temperature cannot exceed the temperature of the FC ($T_{\max} \leq T_{FC}$), and the outflow air is cooled down to an ambient temperature ($T_{\min} = T_{amb}$) before leaving the WRS. In that case, the part of condensed water (k) that can be extracted from the total amount of water circulating in the system may be found from the following equation:

$$k = \frac{\dot{m}_{H_2O}^{coll}}{\dot{m}_{H_2O}^{prod}} \cdot 100\% = \frac{\gamma - 1}{\gamma} \cdot 100\% \tag{19}$$

The graph of k for various ventilation stoichiometries and ambient temperatures is presented in Figure 4. For ambient temperatures lower than −20 °C, the rate of water collection is above 95% even with $\lambda = 10$. For temperatures higher than 0 °C, the ventilation stoichiometry significantly affects water collection parameters. As mentioned above, the ventilation air that enters the WRS also contains a certain amount of water vapor ($m_{H_2O}^{in} > 0$), that was not considered during the analytical calculations; however, it was taken into account during the experiment. Thus, the values of k presented in Figure 4 are an underestimation of the real case.

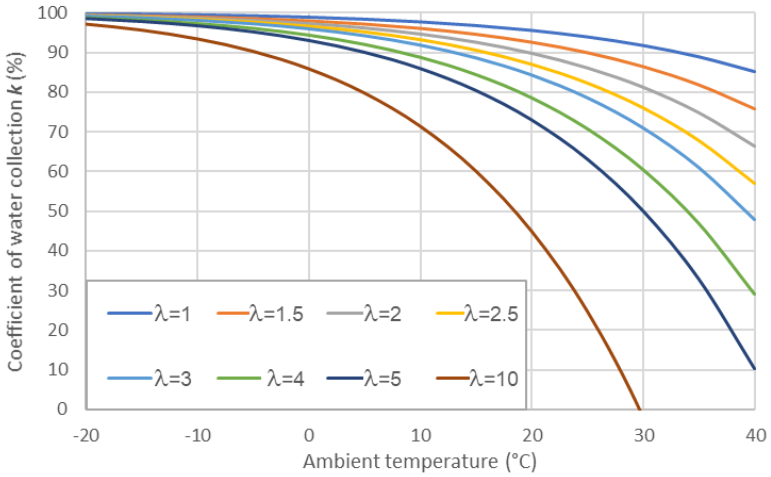

Figure 4. The part of condensed water from water circulating in the system (k), as calculated for various ambient temperatures (T_{amb}) and stoichiometries λ.

Using the above analytical estimation, an experimental study was conducted to present the actual implementation and feasibility of the suggested WRS in the worst-case conditions of room temperature and dry ventilation.

3. Experimental Model

3.1. Experimental Methods

A description of the experimental setup is presented in Figure 5. The system includes a PEMFC placed in a WRS as described below. A 300 W PEMFC with graphite bipolar plate (BPPs) (30xMP-0.01, InEnergy LLC, Moscow, Russia) was supplied with Hydrogen from a compressed tank with a constant pressure of 0.5 bar. The hydrogen flow rate was measured using a digital gas mass flow meter (LIMS-2SLPM, Alicat Scientific, Inc, Tucson, AZ, USA). The FC power output was controlled by a programmable DC load (model 8502, B&K Precision Corp., Yorba Linda, CA, USA) for working at output power conditions of 0–100 W (Figure 5b).

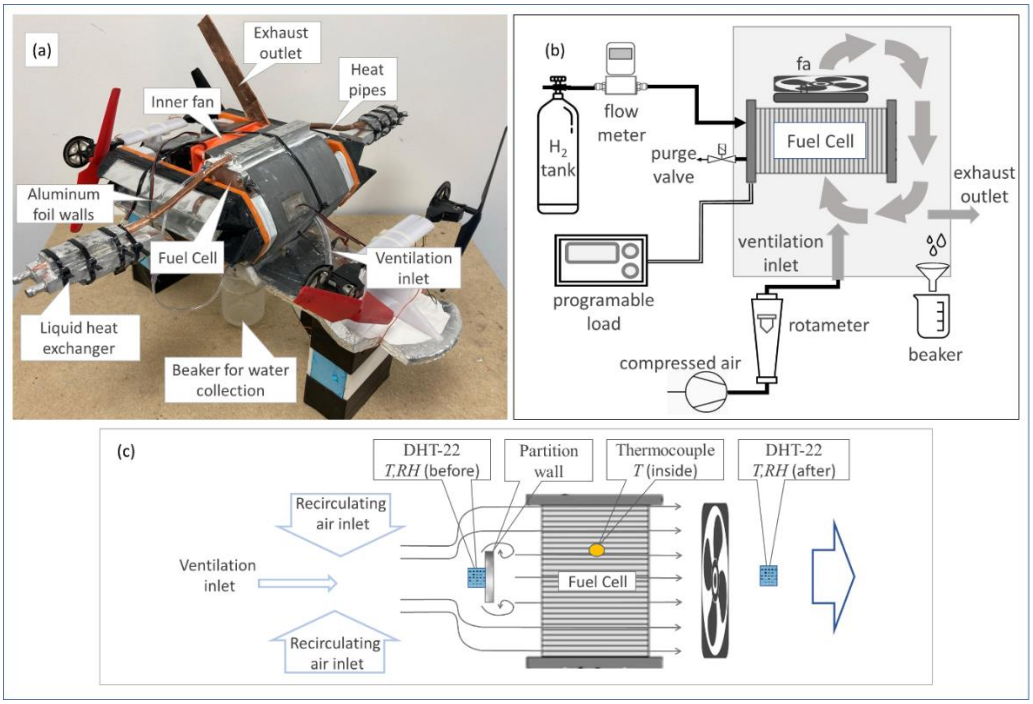

Figure 5. The experimental setup: a representing photo (**a**) and a schematic description (**b**), including the fuel cell enclosed inside a circulating dome with a fan, a ventilation inlet and exhaust outlet, Hydrogen supply, programmable load, flowmeters, and the collecting beaker. Temperature and humidity sensors were placed before and after the FC and a thermocouple was mounted inside the FC (**c**).

The FC was placed inside a 3D-printed WRS dome that resembles a front part of a fixed-wing drone fuselage (Figure 5a). The dome's internal geometry was designed to direct the condensed water to five drain tubes installed at the bottom and ended in a collecting beaker that was placed below the FC. Some of the side sections' walls were made of thick aluminum foil to increase the heat transfer between the ambient flow (simulated by four fans installed at the front and back sides) and the circulating flow inside the WRS dome. The whole system was sealed using silicone glue, except for the two aluminum foil walls that were removable to allow system drying after the experiments. They were attached to the rest of the WRS using rubber film, allowing sufficient isolation.

The air inside the WRS was circulated using an internal fan (12V DC, 12 cm diameter). For the ventilation inlet, significantly dehumidified compressed air at room temperature (20–25 °C) and constant AH of 5 g/m^3 was driven through the inlet port installed in the

nose part at controllable flow rates. The ventilation inlet airflow was measured using an air rotameter (LZT-6T, Barry Century, China) with 0.5 L/min resolution. At the exhaust outlet, a thin copper channel with a 25 cm length and 3 mm × 3.5 cm cross-section was installed as a heat exchanger. To assure steady conditions inside the system, temperature and RH were measured before and after the FC using thermocouples (k-type) and DHT-22 sensors (Figure 5c) connected to an A/D sampling microcontroller (CH340 ATmega328 nano V3).

To simulate the principle of edge cooling by ambient air convection (Figure 6a), the FC temperature regulation in the experiment was implemented using four heat pipes (Figure 6b) that were attached by aluminum connectors to the stack's edges from one side and to water-cooled heat exchanger from their other side. The heat of the coolant water was removed by two Peltier elements TEC1-12710 installed on heat sinks with fans (Figure 6b). All the thermal connections were glued using thermal plaster STARS-922 with thermal conductivity of 0.671 W/(m·K). An Arctic thermal pad with 1.5 mm thickness and thermal conductivity of 6 W/(m·K) was installed between the stack edges and the heat pipe connector to prevent stack short-cutting. This method of cooling was firstly tested without the WRS and revealed satisfying efficiency.

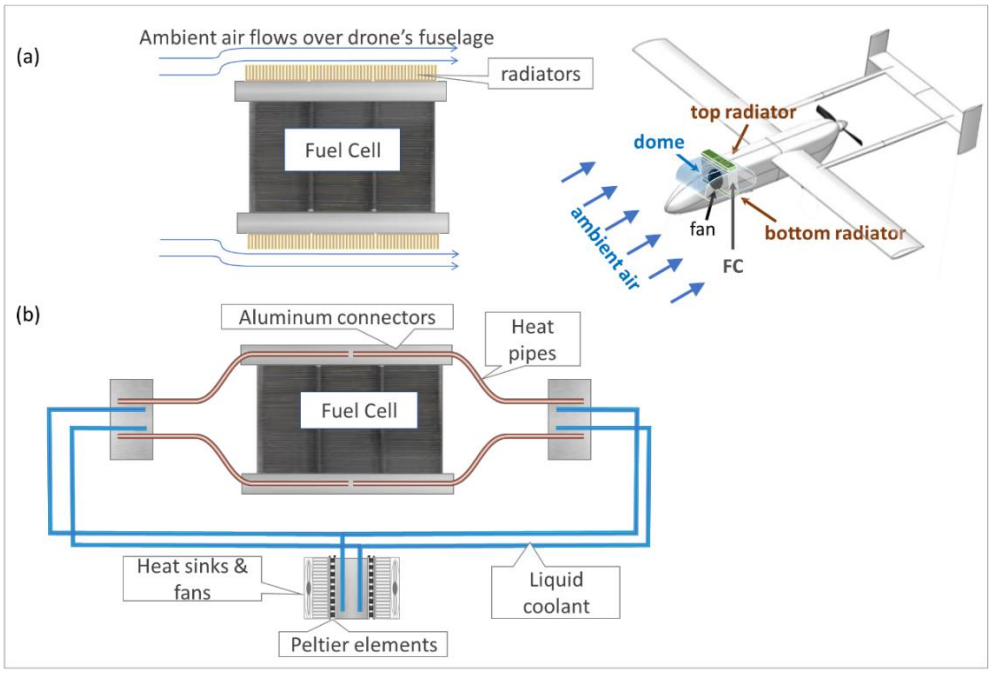

Figure 6. The designed FC edge cooling for UAV, based on convection by ambient air (**a**) as was simulated in the experiments using heat pipes and liquid cooling (**b**). The coolant liquid is cooled down by Peltier elements with an attached heat sink and fans.

3.2. Experimental Results

Before connecting the WRS, the FC was tested under standard operating conditions (open to ambient air, cooled down by an attached fan) to learn its reference parameters. The measured polarization curve of the stack for current up to I = 7 A is presented in Figure 7.

A total of six experiments with the WRS at different power outputs were performed to define the practical ranges of λ, measure the obtained relative amount of condensed water (k), and examine the FCs power output stability for 60 minutes in each case. An example of the measured temperature and humidity before and after the FC during the experiment (for the case with I = 4 A and V_{air} = 14 L/min) is shown in Figure 8. Figure 9 shows the measured FC power outputs for each of the six experiments as a function of time.

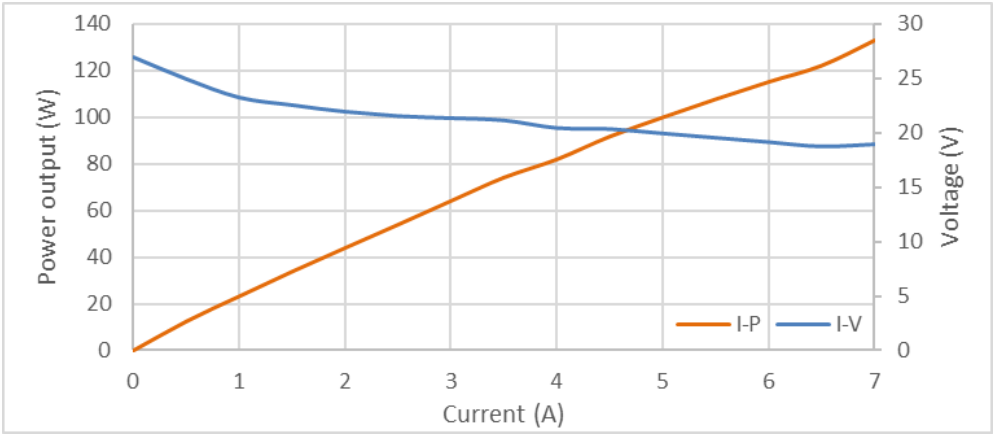

Figure 7. Polarization curves (Voltage and power as a function of current) of the PEMFC, as measured without a WRS.

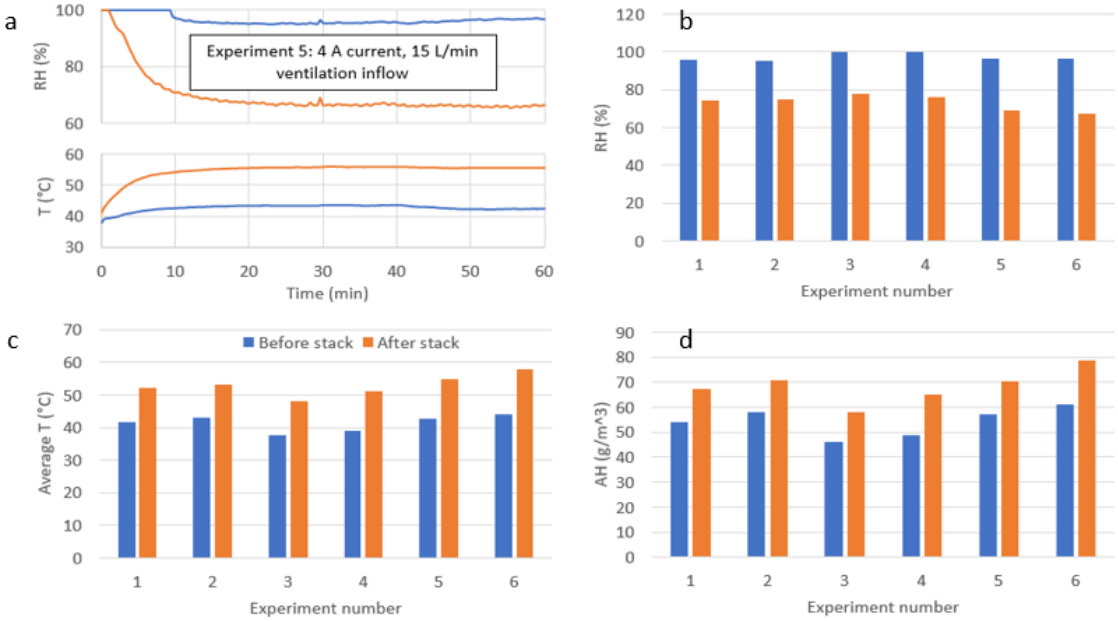

Figure 8. (**a**) A typical variation of temperatures and humidity measured before (blue lines) and after the FC (orange lines) with time. In this case, the operating current was I = 4 A, and the hydrogen flow was V_{air} = 15 L/min. (**b**–**d**) display the average air temperature and relative and absolute humidity recorded before (blue) and after (orange) the FC.

Measurements of stacks inflow and outflow RH and temperature for each experiment reveal the heating process during the first 7–12 min (Figure 8a). It may be due to changes in water balance inside the FC membranes caused by changes in the stacks temperature and ambient humidity. This results in a slight power output decrease within the first ten minutes of operation for most of the experiments (Figure 9). After a steady-state condition was attained inside the WRS, the FC power output was relatively stable, with a minor decrease in power over time (of <3%) of the experiments at I = 4 A and I = 5 A. During a steady-state process, the temperature difference of air before and after the stack was always about 10 °C (for all the cases) as shown in Figure 8c. Detailed results and measurements for the six experiments are summarized in Table 1. For varying cases with obtained power of 20–106 W with ventilation stoichiometries in the range of λ = 2.1–2.5 the achieved coefficient of water collection, k, was relatively constant (51–60%), which is 70–85% of the theoretical amounts of available water for collection.

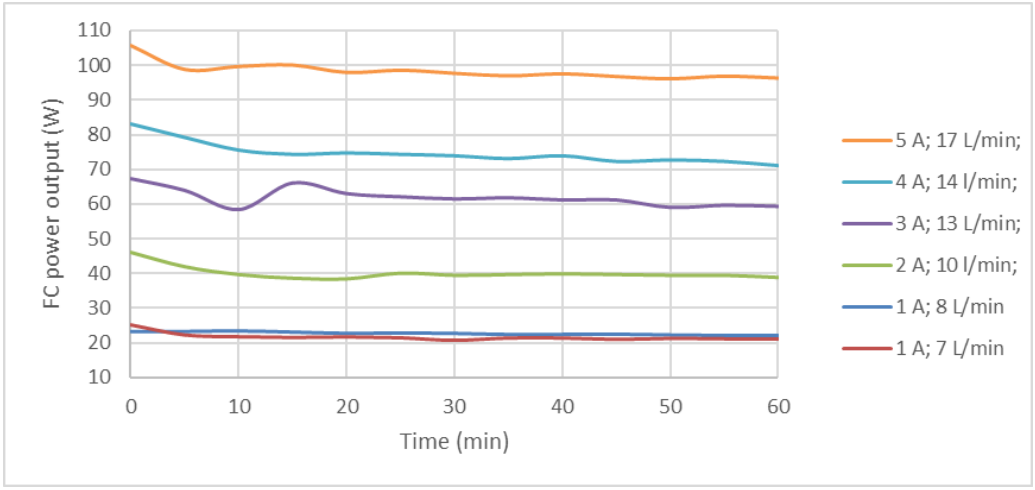

Figure 9. The measured power as a function of time for the different cases with varying currents and ventilation flow rates.

Table 1. Details of the experiments data and results.

Experiment	1	2	3	4	5	6
Stack's average power (W)	23 ± 0.4	20 ± 1	40 ± 1.4	67 ± 2.4	74 ± 5.2	106 ± 2.5
Stack's current (A)	1	1	2	3	4	5
Air inflow (L/min)	8 ± 0.25	7 ± 0.25	10 ± 0.25	13 ± 0.25	15 ± 0.25	17 ± 0.25
Air outflow (L/min) *	7.6	6.5	9.4	12.2	14.2	16.1
Hydrogen flow (L/min)	0.6 ± 0.01	0.6 ± 0.01	0.78 ± 0.02	0.99 ± 0.03	1.12 ± 0.02	1.3 ± 0.02
Ventilation air stoichiometry (λ) **	2.4	2.1	2.4	2.4	2.5	2.4
Average ambient temperature (T_{amb})	26.9 ± 0.21	27.4 ± 0.17	25 ± 0.023	24.7 ± 0.42	25.7 ± 0.18	26.7 ± 0.2
AH at saturation for given T_{amb} (g/m^3)	25.4	26.1	23.1	22.5	23.8	22.1
The expected amount of collected water (g) **	30.7	29.6	38.3	49.1	65.0	64.8
The actual amount of collected water (g)	22	25.2	27.7	40.8	48.5	52.9
Ratio Actual to Expected (%)	71.8	85.3	72.4	83.1	74.6	81.6
Expected coefficient of water collection k (%)	72.75	70.64	70.53	70.65	72.38	71.05
Achieved coefficient of water collection k (%)	52.13	60.14	51.01	58.71	54.01	58.00
GHSC of fuel for achieved k (wt%)	5.3	5.5	5.3	5.5	5.3	5.4

* Calculated using Equation (15); ** The specific equations used for calculations are shown in the Appendix A.

Out of the six cases, the highest relative amount of collected water (85.3% of the theoretical $\dot{m}_{H_2O}^{coll}$) was achieved during the second experiment with the lowest ventilation stoichiometry of λ = 2.1. However, the average power output of the stack was lower than during the first attempt performed with the same constant current of 1 A (20 W vs. 23 W); this may imply that in this setup, λ = 2.1 is a minimal value, and thus λ ≥ 2.4 was specified for the other cases. In the fourth attempt with I = 3 A and λ = 2.4, 83.1% of the theoretical amount of water was collected. The achieved coefficient of water collection k was 58.8%, which means that even for the relatively high ambient temperature (25–27 °C) and dry inlet air, more than half of all the water that entered the system was collected.

These results may be translated (using Equation (8)) to the theoretical average fuel energy density of GHSC = 5.3–5.5 wt% for the different cases. These values are expected to become even more significant for lower ambient temperatures and humid inlet air.

4. Discussion

In this paper, we studied a new method of water recuperation from open-cathode PEMFC. We developed the corresponding theoretical calculations defining the operation conditions and an experimental setup to validate the concept feasibility under worst-case conditions of room ambient temperatures and dry inlet ventilation.

The suggested WRS with circulation and controlled ventilation ports may allow both sufficient oxygen supply through ventilation to support FCs' stable operation and the conditions for vapor condensation inside the dome. The ventilated airflow may be supplied either by a pump or regulated air intake if such a system is utilized on a fixed-wing drone.

Usual commercially available open cathode PEMFCs are designed to operate at high ventilation flow rates while the cooling flow greatly exceeds the stoichiometric amount of air required for stable operation. For example, for a commercial stack with 35 MEA BPP operating at 100 W and 5 A is about 3 L/min (estimated using Equation (12)), the typical colling fan (e.g., Noctua NH-U9S) may provide an average flow of 1000 L/min, which results in stoichiometry $\lambda > 300$. According to the theoretical analysis presented here, to maximize the water collection by the WRS, the ventilation inflow should be decreased to the minimal amount sufficient for FC stable operation (Figure 3). However, if a ventilation flow at low temperature and low stoichiometry is supplied directly to an open-cathode PEMFC, it may cause water condensation inside the stack due to changed water balance in the MEAs, which in turn might cause cathode flooding and stack operation failure. Thus, the flow through the stack itself must be high enough to sustain proper water balance, while ventilation stoichiometry should be as low as possible. Moreover, ventilation is inevitably associated with the outflow of humid used air and therefore reduces the water utilization inside the dome.

Indeed, the experiments revealed that while the ventilation flow rate is kept at $\lambda > 2.4$, the FC operation is stable for a relatively long duration (60 min) while placed inside a semi-closed system. Even with a relatively high ambient temperature of 25–27 °C and dry inlet ventilation, the air circulation, edge cooling, and controlled ventilation allowed for a constant rate of condensation and collection of more than half of the water entered the system (from the FC and ventilation). This suggested method may be implemented in systems that use water as a fuel for light on-demand hydrogen generators (e.g., SBH-based) and thus can increase the average fuel's energy density associated with SBH to GHSC of 6.8 wt% and can be further increased if byproduct emission is applied.

With emission, the system's weight will decrease during operation and overall efficiency will improve. The expected flight time for the UAV, in that case, might be found to be similar to the Breguet range/flight time equation:

$$t = \frac{1}{\chi \cdot SFC} \ln\left(\frac{W_{initial}}{W_{final}}\right) \quad (20)$$

where χ is the drone's specific power required for a cruise flight measured in kW/kg, SFC is propulsion system-specific fuel consumption measured in kg/kWh and $W_{initial/final}$ are the drone's initial and final weights.

To illustrate the increase in flight duration for a such system with recuperation and byproduct emission, let us consider a study performed by Lapena-Rey et.al. [26] who performed an experimental test of SBH solution-based power pack with a 200 W FC (AEROPACK) installed on 11 kg maximal take-off weight fixed-wing drone and measured the real fuel consumption and required power for cruise flight. For the studied case, the fuel mass was 1 kg, which corresponds to the 1 L volume of 20 wt% SBH solution. This is similar to the ratio of the generator developed by our research group. The main difference is that we use a solid SBH solution, which is on-demand mixed with water and catalyst instead of a premixed solution. The fuel consumption was about 210 g/h at an average power output of 194 W. Assuming SFC as a linear function of power in the limited FC operational range (see Supplementary Material), calculation using Equation (20) reveals a 53% increase in flight duration from 4.7 to 7.2 h with 90% water recuperation (for 1 kg fuel,

as described in [26]) and 60% from 4.7 to 7.5 h with recuperation and emission. Moreover, if the same system would store 4 kg of fuel out of a 11 kg maximal take-off weight, then the increase in cruise flight duration and, accordingly, the range would reach 100% (from 18 to 38 hours). That way, utilization of recuperated water along with byproducts emission reveals a great opportunity to develop long-range lightweight aircraft.

The actual amount of collected water in the experiments is relatively close (70–85%) to the expected amount of collected water calculated by the theoretical model (Table 1). The differences between the experimental measurements and the theoretical estimations might be caused by the following factors.

Despite the satisfying heat removal rate achieved by using the edge cooling method, inhomogeneous temperature distribution of the stack is revealed during operation (Figure 10a) with differences of up to 12 °C. The stacks' temperature was measured by a single k-type thermocouple placed where the highest temperatures were found by a thermal camera during cooling system testing without WRS (Figure 10a). Moreover, during the experiments with the WRS, the temperatures measured inside the FC (using the thermocouple mounted inside the stack, shown in Figure 5c) were lower than the temperatures measured for the stacks outflow (using the DHT, shown in Figure 5c), indicating non-homogenous temperature distribution in the stack.

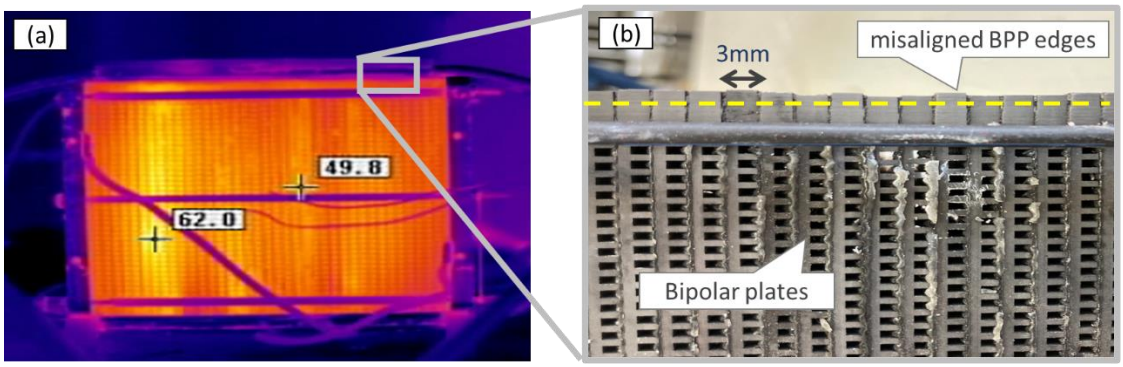

Figure 10. (**a**) Temperature distribution of the edge-cooled FC (in a case without WRS); (**b**) magnified side view of the utilized PEMFC with graphite bipolar plates showing BPP edges misalignment.

Most probably, this was caused by the stack's edges unevenness. The height difference between two neighboring BPPs was up to 2 mm (Figure 10b), which resulted in differences in heat removal rates for each BPP.

During experiments, we were able to reveal extra hydrogen consumption conjugated with FC heating even with no load applied. This indicates membrane damage: some hydrogen might flow through it and react with oxygen on the catalyst layer of the cathode side. Most probably, such damage is a result of the FC's local overheating caused by the inhomogeneous temperature distribution. Such a reaction, however, also goes with water production. Therefore, the total theoretical amount of produced water was calculated using the measured hydrogen flow rate. A part of the hydrogen, however, might have left the system through the exhaust without reaction.

This combined issue of membrane overheating, and hydrogen leakage is expected to be solved by using FC stacks with flat edges, more accurate temperature control, and a better mixing between the ventilation and recirculating flow.

Another possible reason for the FC local overheating (hot spots) may be uneven oxygen distribution in the airflow entering the stack since the ventilation inlet was situated directly in front of the stack's center (Figure 5c). The partition wall utilized during the experiment was designed to improve flow mixing and make oxygen distribution more homogenous, but it is hard to estimate the efficiency of such a solution.

In addition, some insignificant water may be absorbed by the FC and released through the H_2 exhaust port. A part of the water that diffuses to the anode part of the MEA due to

electro-osmosis [27], saturated the H_2 inside the stack and left the system with the FC H_2 exhaust (the valve opened once in a minute for one second). The amount of this water was not measured, but it is expected to be much lower than the amount of recuperated water. For the actual onboard system, this water might be recuperated if the purged H_2 is released through the WRS exhaust.

Additional possible reasons for discrepancies from theory may include drainage system imperfection (i.e., part of the condensed water remained inside the WRS), possible leakage of humid air through the system's wall without passing the heat exchanger, and some humid exhaust air left the system (through the heat exchanger) before cooling down to ambient temperature (it, however, was checked several times during each experiment by inserting the thermocouple to the heat exchanger).

Despite those limitations, a stable FC performance was observed inside a semi-closed system in all the examined cases (Figure 9), and the obtained experimental measurements for water recuperation are in fair agreement with the theoretical calculations (Table 1).

Additional cooling of circulating air by the aluminum foil walls (Figure 5a) assisted in preventing over-humidifying of the MEAs in the stack. The condensation process was stable and water dripping was observed from all the parts of the system. Drainage might be improved by applying hydrophobic–hydrophilic patterns to the inner walls of the system [28,29].

The obtained theoretical energy density of the fuel in the experiments with worst-case conditions reached GHSC > 5.5 wt% (Table 1). When high altitudes are considered with lower ambient temperatures and with product emission, these values are expected to become even more significant (Figure 2) with up to GHSC = 6.8 wt% for stored fuel. In addition to that, the emission of reaction products will further increase overall efficiency, depending on the relative weight of the fuel in the aircraft.

5. Conclusions

The water harvesting method suggested in this work has the potential to significantly increase the energy density of hydrogen generators based on the hydrolysis of solid hydride by water. In certain combinations of the system (e.g., using a lightweight FC stack and a cooling system, combined with an efficient generator with a relatively high amount of stored fuel and products emission), it may be possible to reach the target of hydrogen storage set to 5.4 wt% by 2025 with a safely stored, easily operated, and on-demand hydrogen generation system. Specifically, the described method may be applied for water recuperation on a UAV, where the FC should be separated from the dry and cold ambient air. The complete power pack system requires further design efforts: in the described experimental system, the condensed water was collected by the glass beaker situated under the cell. Such an approach could easily be employed for multi-rotor UAVs, which allow for the vertical alignment of a recuperated water reservoir placed under the WRS. However, the challenge of FC cooling in such a case needs to be further explored. When a fixed-wing UAV with an integrated FC is considered, we showed in a previous study [19] that radiators attached to the fuselage (Figure 6a) are sufficient to allow FC edge cooling by convection for flight speeds >10 m/s. Yet, in this case, the shape of the WRS should be modified to funnel all the condensed water to one location inside the system.

In the future, we plan to build a similar experimental system with a more suitable fuel cell that has flat edges and a control system which prevents overheating. Hence, longer operation periods and various ambient conditions may be examined. Another step will be to develop a complete energy delivery system based on the combined WRS and Hydrogen generator with SBH as a hydrogen-stored energy source in a compact power pack.

Supplementary Materials: The following supporting information can be downloaded at: https://www.mdpi.com/article/10.3390/en15186848/s1, supplementary materials presented in tabular form.

Author Contributions: Conceptualization, A.S., I.A. and L.Z.; methodology, validation, investigation, software and formal analysis, L.Z.; writing—original draft preparation, L.Z. and I.A.; writing—review

and editing, A.S., I.A. and L.Z.; visualization, I.A.; supervision, I.A. and A.S.; project administration, L.Z. and I.A.; funding acquisition, I.A.; resources I.A. and A.S. All authors have read and agreed to the published version of the manuscript.

Funding: This study was funded by a grant from the Israeli Ministry of Energy (grant number: 219-11-136).

Data Availability Statement: The calculation of SFC for various k can be found in the supplementary material.

Acknowledgments: The authors would like to thank Mordechai Kremer, Eyal Hayuk, and Taya Balberg for their contribution and Nir Tsabar for academic support. Lev Zakhvatkin was supported by a scholarship from the Israeli Ministry of Aliyah and Integration and a scholarship of Ariel University graduate studies. Alex Schechter thanks the Planning and Budgeting Committee of the Israel Council for Higher Education (CHE) and the Fuel Choice Initiative (Israeli Prime Minister's Office) within the framework of the Israel National Research Center for Electrochemical Propulsion (INREP).

Conflicts of Interest: Authors declare no conflict of interest.

Appendix A

The expected amount of collected water:

$$m_{H_2O}^{expected} = m_{H_2O}^{produced} + m_{H_2O}^{in} - \dot{V}_{out} AH(T_{amb})t$$
$$m_{H_2O}^{produced} = \frac{\dot{V}_{H_2}\rho_{H_2}}{M_{H_2}} M_{H_2O} t.$$
$$m_{H_2O}^{in} = AH_{in}\dot{V}_{vent}t$$
$$AH_{in} = 0.005\ \left(\tfrac{g}{L}\right); t = 60\ min$$

Stoichiometric air inflow for measured hydrogen flow:

$$\dot{V}_{air}^{st} = \dot{n}_{air}^{st}\rho_{air}M_{air};\ \rho_{air} = 1.2\ \left[\tfrac{g}{L}\right];\ M_{air} = 28.97\ \left[\tfrac{g}{mol}\right]$$
$$\dot{n}_{air}^{st} = \frac{\dot{n}_{H_2}^{st}}{2{\cdot}0.21} = \frac{\dot{V}_{H_2}\rho_{H_2}}{2{\cdot}0.21M_{H_2}};\ \rho_{H_2} = 0.1227\ \left[\tfrac{g}{l}\right]\ at\ 1.5\ pressure\ and\ 25^{\circ}C$$

0.21—a molar fraction of oxygen in the air, $\dot{n}_{air}^{st}$—molar flow.
Produced water:

$$m_{H_2O} = t{\cdot}\dot{n}_{H_2O}M_{H_2O} = t{\cdot}\dot{n}_{H_2}M_{H_2}$$

References

1. Graetz, J. New approaches to hydrogen storage. *Chem. Soc. Rev.* **2009**, *38*, 73–82. [CrossRef] [PubMed]
2. Züttel, A. Materials for hydrogen storage. *Mater. Today* **2003**, *6*, 24–33. [CrossRef]
3. Sun, C.; Zhang, H. Review of the Development of First-Generation Redox Flow Batteries: Iron-Chromium System. *ChemSusChem* **2022**, *15*, e202101798. [CrossRef] [PubMed]
4. Godula-Jopek, A.; Westenberger, A.F. FC Types: PEMFC/DMFC/AFC/PAFC//MCFC/SOFC/. *Encycl. Energy Storage* **2022**, *2*, 250–265. [CrossRef]
5. Lü, X.; Miao, X.; Liu, W.; Lü, J. Extension control strategy of a single converter for hybrid PEMFC/battery power source. *Appl. Therm. Eng.* **2018**, *128*, 887–897. [CrossRef]
6. Demirci, U.B.; Akdim, O.; Andrieux, J.; Hannauer, J.; Chamoun, R.; Miele, P. Sodium Borohydride Hydrolysis as Hydrogen Generator: Issues, State of the Art and Applicability Upstream from a Fuel Cell. *Fuel Cells* **2010**, *10*, 335–350. [CrossRef]
7. Available online: https://www.energy.gov/eere/fuelcells/doe-technical-targets-onboard-hydrogen-storage-light-duty-vehicles (accessed on 1 September 2022).
8. Rivard, E.; Trudeau, M.; Zaghib, K. Hydrogen Storage for Mobility: A Review. *Materials* **2019**, *12*, 1973. [CrossRef]
9. Barthelemy, H.; Weber, M.; Barbier, F. Hydrogen storage: Recent improvements and industrial perspectives. *Int. J. Hydrog. Energy* **2017**, *42*, 7254–7262. [CrossRef]
10. Tarhan, C.; Çil, M.A. A study on hydrogen, the clean energy of the future: Hydrogen storage methods. *J. Energy Storage* **2021**, *40*, 102676. [CrossRef]
11. Hassan, I.; Ramadan, H.S.; Saleh, M.A.; Hissel, D. Hydrogen storage technologies for stationary and mobile applications: Review, analysis and perspectives. *Renew. Sustain. Energy Rev.* **2021**, *149*, 111311. [CrossRef]

12. Kim, J.-H.; Lee, H.; Han, S.-C.; Kim, H.-S.; Song, M.-S.; Lee, J.-Y. Production of hydrogen from sodium borohydride in alkaline solution: Development of catalyst with high performance. *Int. J. Hydrog. Energy* **2004**, *29*, 263–267. [CrossRef]
13. Amendola, S.C.; Sharp-Goldman, S.L.; Janjua, M.; Kelly, M.T.; Petillo, P.J.; Binder, M. An ultrasafe hydrogen generator: Aqueous, alkaline borohydride solutions and Ru catalyst. *J. Power Sources* **2000**, *85*, 186–189. [CrossRef]
14. Nunes, H.; Ferreira, M.; Rangel, C.; Pinto, A. Hydrogen generation and storage by aqueous sodium borohydride ($NaBH_4$) hydrolysis for small portable fuel cells (H_2–PEMFC). *Int. J. Hydrog. Energy* **2016**, *41*, 15426–15432. [CrossRef]
15. Marchionni, A.; Bevilacqua, M.; Filippi, J.; Folliero, M.G.; Innocenti, M.; Lavacchi, A.; Miller, H.A.; Pagliaro, M.V.; Vizza, F. High volume hydrogen production from the hydrolysis of sodium borohydride using a cobalt catalyst supported on a honeycomb matrix. *J. Power Sources* **2015**, *299*, 391–397. [CrossRef]
16. Zakhvatkin, L.; Zolotih, M.; Maurice, Y.; Schechter, A.; Avrahami, I. Hydrogen Production on Demand by a Pump Controlled Hydrolysis of Granulated Sodium Borohydride. *Energy Fuels* **2021**, *35*, 11507–11514. [CrossRef]
17. Fujinuma, S.; Ashida, S.; Hoshi, N. Basic Study for Model Construction of The Water Recovery System in Polymer Electrolyte Fuel Cells. In Proceedings of the 2018 7th International Conference on Renewable Energy Research and Applications (ICRERA), Paris, France, 14–17 October 2018; pp. 938–943. [CrossRef]
18. Tibaquirá, J.E.; Hristovski, K.D.; Westerhoff, P.; Posner, J.D. Recovery and quality of water produced by commercial fuel cells. *Int. J. Hydrog. Energy* **2011**, *36*, 4022–4028. [CrossRef]
19. Anand, N.; Raja, M.; Rangaswamy, T. Passive Liquid Water Recovery from Fuel Cell Exhaust. *Int. J. Recent Res. Civ. Mech. Eng. (IJRRCME)* **2014**, *1*, 18–23. Available online: https://www.paperpublications.org (accessed on 1 September 2022).
20. De Las Heras, A.; Vivas, F.; Segura, F.; Redondo, M.; Andújar, J. Air-cooled fuel cells: Keys to design and build the oxidant/cooling system. *Renew. Energy* **2018**, *125*, 1–20. [CrossRef]
21. Ustolin, F.; Taccani, R. Fuel cells for airborne usage: Energy storage comparison. *Int. J. Hydrog. Energy* **2018**, *43*, 11853–11861. [CrossRef]
22. Gadalla, M.; Zafar, S. Analysis of a hydrogen fuel cell-PV power system for small UAV. *Int. J. Hydrog. Energy* **2016**, *41*, 6422–6432. [CrossRef]
23. Zakhvatkin, L.; Schechter, A.; Buri, E.; Avrahami, I. Edge Cooling of a Fuel Cell during Aerial Missions by Ambient Air. *Micromachines* **2021**, *12*, 1432. [CrossRef] [PubMed]
24. Bhosale, A.C.; Ghosh, P.C.; Assaud, L. Preparation methods of membrane electrode assemblies for proton exchange membrane fuel cells and unitized regenerative fuel cells: A review. *Renew. Sustain. Energy Rev.* **2020**, *133*, 110286. [CrossRef]
25. Sun, C.; Zhang, H. Investigation of Nafion series membranes on the performance of iron-chromium redox flow battery. *Int. J. Energy Res.* **2019**, *43*, 8739–8752. [CrossRef]
26. Lapeña-Rey, N.; Blanco, J.; Ferreyra, E.; Lemus, J.; Pereira, S.; Serrot, E. A fuel cell powered unmanned aerial vehicle for low altitude surveillance missions. *Int. J. Hydrog. Energy* **2017**, *42*, 6926–6940. [CrossRef]
27. Dai, W.; Wang, H.; Yuan, X.-Z.; Martin, J.J.; Yang, D.; Qiao, J.; Ma, J. A review on water balance in the membrane electrode assembly of proton exchange membrane fuel cells. *Int. J. Hydrog. Energy* **2009**, *34*, 9461–9478. [CrossRef]
28. Ji, X.; Zhou, D.; Dai, C.; Xu, J. Dropwise condensation heat transfer on superhydrophilic-hydrophobic network hybrid surface. *Int. J. Heat Mass Transf.* **2019**, *132*, 52–67. [CrossRef]
29. Yang, K.-S.; Lin, K.-H.; Tu, C.-W.; He, Y.-Z.; Wang, C.-C. Experimental investigation of moist air condensation on hydrophilic, hydrophobic, superhydrophilic, and hybrid hydrophobic-hydrophilic surfaces. *Int. J. Heat Mass Transf.* **2017**, *115*, 1032–1041. [CrossRef]